

Natural convection heat transfer in a cavity filled with electrically conducting nano-particle suspension in the presence of magnetic field

Cite as: Phys. Fluids 31, 023302 (2019); <https://doi.org/10.1063/1.5080778>

Submitted: 12 November 2018 . Accepted: 10 January 2019 . Published Online: 05 February 2019

Desh Deepak Dixit, and Arvind Pattamatta



View Online



Export Citation



CrossMark

PHYSICS TODAY
WHITEPAPERS

ADVANCED LIGHT CURE ADHESIVES

Take a closer look at what these environmentally friendly adhesive systems can do

READ NOW

PRESENTED BY
MASTERBOND
PATENTED | SEALANTS | COATINGS



Natural convection heat transfer in a cavity filled with electrically conducting nano-particle suspension in the presence of magnetic field

Cite as: Phys. Fluids 31, 023302 (2019); doi: 10.1063/1.5080778

Submitted: 12 November 2018 • Accepted: 10 January 2019 •

Published Online: 5 February 2019



Desh Deepak Dixit and Arvind Pattamatta^{a)}

AFFILIATIONS

Heat Transfer and Thermal Power Laboratory, Department of Mechanical Engineering, Indian Institute of Technology Madras, Chennai 600036, India

^{a)} Author to whom correspondence should be addressed: arvindp@iitm.ac.in. Tel.: +91 44 2257 4654. Fax: +91 44 2257 4652.

ABSTRACT

This work reports the effect of uniform magnetic field on the heat transfer behavior in the natural convection of electrically conducting but non-magnetic nano-particle suspensions. The experiments are carried out in a differentially heated cubical cavity with two opposite vertical faces at a different uniform temperature kept in a uniform magnetic field. The Rayleigh number range for the present experiment is between 1×10^6 and 1×10^7 . To investigate the effect of volume fraction and the type of nanofluid, three different volume fractions of multi-wall carbon nanotubes, graphene, copper, and silica nanofluid are tested at different strengths and directions of the magnetic field. The presence of magnetic field deteriorates the heat transfer which depends upon the direction, strength of the magnetic field and type, and volume fraction of the nanofluid used. The role of magnetic field in the suppression of heat transfer in the presence of magnetic field is explained by a theory involving the interaction of moving electrically conducting particles with the uniform magnetic field.

Published under license by AIP Publishing. <https://doi.org/10.1063/1.5080778>

NOMENCLATURE

A	area of cross section, m^2
B	magnetic field, T
C	specific heat capacity, J/kg K
E	electric field, N/C
F	Lorentz force, N
g	acceleration due to gravity, m/s^2
h	convective heat transfer coefficient, $W/m^2 K$
I	current, A
\hat{i}	unit vector along the X-direction
J	current density, A/m^2
\hat{j}	unit vector along the Y-direction
k	thermal conductivity, $W/m K$
\hat{k}	unit vector along the Z-direction
L	side of the cubical cavity, m
Nu	Nusselt number
Q	heat rate, W
Ra	Rayleigh number

T	temperature, K
\vec{V}	velocity, m/s
V	voltage, V

Greek letters

α	thermal diffusivity, m^2/s
β	coefficient of thermal expansion (1/K)
μ	dynamic viscosity, kg/m s
ν	kinematic viscosity, m^2/s
ρ	density, kg/m^3
σ	electrical conductivity, S/m
ϕ	volume fraction
Ω	volume, m^3

Subscripts

bf	base fluid
np	nano-particle
nf	nanofluid

w	water
x	X direction
y	Y direction
z	Z direction

Abbreviation

DI	de-ionised
DC	direct current
MWCNT	multi-wall carbon nanotubes
SDS	sodium dodecyl sulfate

I. INTRODUCTION

Removal of heat from systems to keep their temperature in operating conditions is a challenge. In this regard, the natural convection heat transfer is one of the most common solutions, in which density difference causes bulk motion of the fluid. To enhance the heat transfer in natural convection, various fluids from mineral oils to liquid metals are used: nanofluid is one such fluid. Nanofluid is a suspension of particles (<100 nm) uniformly dispersed in a base fluid. The nanofluid possesses higher thermal conductivity and the non-settling, non-clogging property makes it a possible choice for coolant. In order to address the challenge of removing high heat flux from a micro-channel, Choi used nanofluid as a coolant.¹ A plethora of nanofluid applications such as in solar collector,² electronic cooling,³ and cooling of nuclear reactors⁴ have been suggested.

Studies on natural convection with nanofluids have been a key area of interest for many researchers worldwide. Researchers have been reporting results ranging from enhancement to deterioration of heat transfer in natural convection with nanofluids. Choi investigated the natural convection (Rayleigh Benard) theoretically in nanofluids and found out that the nanofluid has a higher heat transfer coefficient in his study.⁵ Nnanna *et al.*⁶ experimentally investigated natural convection in aluminium oxide-water, copper-ethylene glycol nanofluid and found out that natural convection precludes settling of nano-particles and the heat transfer characteristics of nanofluid are similar to those of the base fluid. Wen and Ding⁷ experimentally investigated transient and steady-state natural convection using TiO₂-water nanofluid, found that heat transfer decreases in both transient and steady-state natural convection, and suggested some possible reasons for the same. Experimental study of Ni *et al.*⁸ in turbulent natural convection in a Rayleigh Benard configuration showed overall deterioration in heat transfer. Joshi and Pattamatta⁹ experimentally investigated alumina/water, multi-wall carbon nanotube (MWCNT)/water, and graphene/water nanofluid and reported an enhancement in heat transfer at an optimum volume fraction for flake and tubular type nano-particle suspension and deterioration for spherical nano-particle suspension. Mohebbi *et al.*¹⁰ studied natural convection within a C-shaped cavity with different locations of the heat source to achieve maximum heat transfer.

With the increased level of complexity and sophistication of modern industries, the interaction of the magnetic field with coolants is unavoidable. The interaction of the magnetic

field with coolant (nanofluid) can perturb the heat transfer in cooling applications where high strength magnetic field is an integral part of the system such as in Magnetic Resonance Imaging¹¹ and fusion reactors.⁴ Thus, the study on the effects of external factors like magnetic field on the heat transfer behavior of the coolant becomes crucial. There have been experimental-numerical studies involving liquid metals¹² and magnetic nano-particle suspensions¹³ and a numerical study on electrically conducting nano-particle suspensions¹⁴ in the presence of magnetic field. The behavior of nano-suspensions with electrically conducting, non-magnetic nano-particles has not been studied experimentally. Very few numerical studies that are present in the literature model the nanofluid to be a homogeneous, single phase fluid and use correlations to model the properties.^{15,16} The existing numerical studies mainly consider effective electrical conductivity of the nanofluid in simulations and solve it using the principles of magneto-hydrodynamics.¹⁷ However, the electrical conductivity of the nanofluid is of very small order to show any significant effect at the magnitude of magnetic field, generally encountered in laboratories or industries.¹⁸ Present experiments are conducted in a differentially heated cubical acrylic cavity with two opposite vertical faces being at two different constant temperatures in the presence of a uniform external magnetic field. Experimental results clearly evince that there is a deteriorating effect of magnetic field on heat transfer even at small values of magnetic field like 0.13 T, which can be explained by considering the electrical conductivity of the particles individually rather than of the fluid as a whole. This approach is useful when the suspended particles possess a high electrical conductivity like copper and graphene, and the fluid surrounding the particle has an electrical conductivity which is negligible with respect to the particle. The heat transfer in the presence of magnetic field is found to be influenced by the direction and strength of the magnetic field, volume and electrical conductivity of the individual particle, and the concentration of the nanofluid. To explain the deterioration of heat transfer, this paper discusses the physics behind the interaction of electrically conducting particles moving in a uniform magnetic field, and the discussed physics justifies the dependence of heat transfer deterioration on the direction and strength of the magnetic field and nano-particle type. The present study also reports the heat transfer behaviour of considered nanofluids in the absence of magnetic field.

II. EXPERIMENTAL SETUP

The schematic of the experimental setup is shown in Fig. 1. The setup for the experiment mainly consists of a test cavity, a cold bath, a DC power source, a data logger, and an electromagnet in between whose poles the test cavity is interjected.

The test cavity consists of the following three sections:

- **Adiabatic (middle) section:** The adiabatic section is made by machining a through square hole (25 mm × 25 mm) in a 25 mm thick, 55 mm × 55 mm acrylic plate and two tapped holes are machined on the top of the

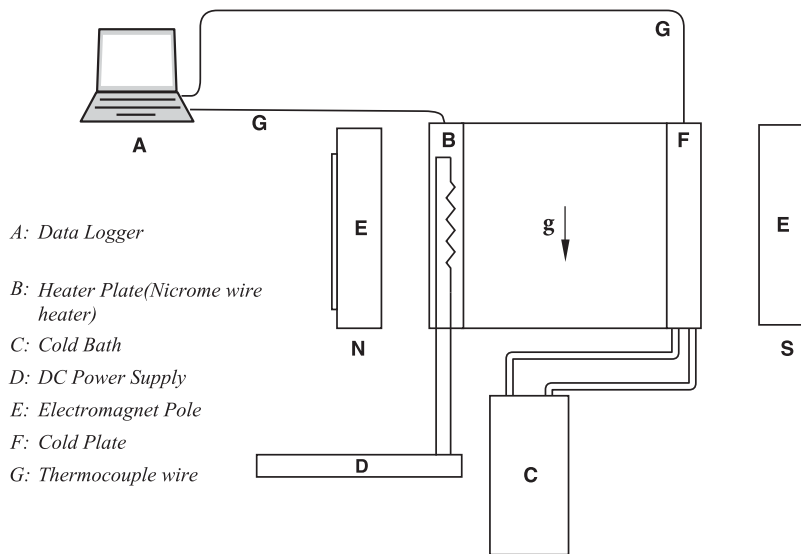


FIG. 1. Schematic of the experimental setup.

section for easy removal and introduction of the test fluid along with the easy removal of air trapped inside the cavity. Two free faces (left and right) of the adiabatic section are closed by the heater and condenser sections.

- **Heater section:** The heater side closes up the one side of the adiabatic (middle) section. It consists of a Teflon coated copper plate with 5 holes on sides for thermo-couple installation and a Nichrome wire electrical heater pasted on its back. The Teflon coated copper plate with the heater pasted on its back is then inserted into an acrylic cover with glass wool insulation in between to reduce the heat loss from the back side of the heater.
- **Condenser section:** Finally, the second bare face of the adiabatic (middle) section is closed using the condenser section. The construction of the condenser section is similar to the heater section. In the condenser

section, a Teflon coated copper plate is inserted into the acrylic cover with the channel machined on it for the flow of constant temperature fluid from the constant water bath.

A photograph of the dismantled cavity is shown in Fig. 2.

All three sections are screwed together using stainless steel bolts with O-rings in between to avoid leakage.

The thermocouples used in experiments are all K-type; all of the thermocouples used in the experiments are calibrated and have an accuracy of $\pm 0.1^\circ\text{C}$. The thermocouples are calibrated from 5.0°C to 80.0°C in steps of 5.0°C ; thereafter, a linear correlation is built using the calibration data for each thermocouple. The correlation obtained is fed into the data-logger for temperature measurement. The calibration of thermocouples is carried out using a Fluke Super-DAQ data acquisition system against a Fluke 5609 PRT (Platinum Resistance Thermometer) probe, a Fluke Dry Well is used as bath

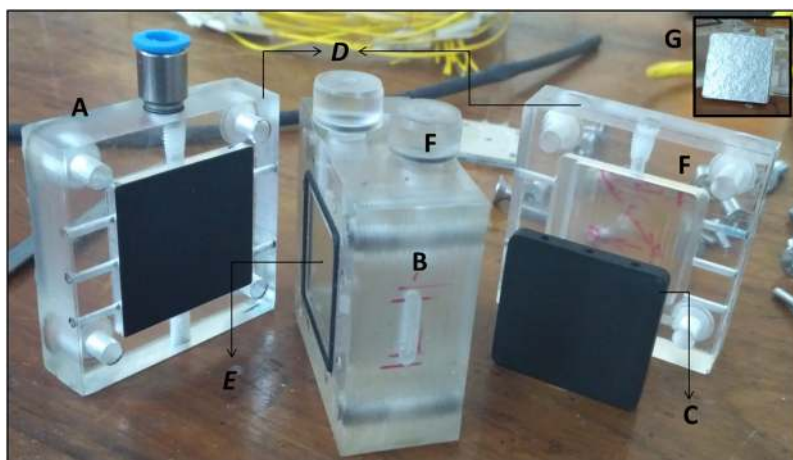


FIG. 2. Photograph of the test section: A. condenser section, B. adiabatic section, C. Teflon coated copper plate, D. acrylic cover plate, E. square through hole (cavity), F. heater section, and G. Nichrome wire heater (sandwiched between mica sheets).

for calibration. To minimize cold junction compensation, the thermocouples were calibrated along with the data-logger at constant ambient temperature. Calibration is carried out at a calibration laboratory of Central Electronics Center [accredited (ISO certified)] at IIT Madras in a controlled environment. The ambient temperature is kept within 25 °C–26.5 °C for all experiments. The data logger used is a product of HIOKI, a Japanese make, which can take temperature readings at the required frequency; in the present experiment, data are recorded as 1 Hz for 120 s. The cold bath used for experiments is manufactured by JULABO (a German make); it can supply water at a constant temperature with a temperature stability of ± 0.01 °C. The electromagnet used in experiments can produce magnetic fields up to 1.0 T (depending upon the pole gap), with $\pm 1\%$ accuracy. To cool the coils of the electromagnet, a separate 30-l cold bath is used.

A. Nanofluid preparation

Present experiments are carried out with four different types of nanofluids with different nano-particle concentrations in DI-water as base fluid. The choice of nano-particles is provided on the basis of the shape of the particle and the electrical conductivity of the nano-particle.

- Multi-Wall Carbon NanoTubes (MWCNTs): MWCNT is chosen for its tubular shape and high electrical conductivity.¹⁹ To investigate the effect of volume fraction on heat transfer, three different volume fractions (0.057%, 0.1%, and 0.2% v/v) of MWCNT are prepared.
- Graphene nano-particle: Mono layered graphene nano-particles are chosen because of their flat-flake structures and very high electrical conductivity.²⁰ Similar to the MWCNT nanofluid, three different volume fractions of graphene nanofluid are prepared for comparison between all nanofluids.

- Copper nano-particle: Copper nano-particles are chosen because of its high electrical conductivity and spherical shape. Copper nanofluid is observed to get oxidized after two days because of dissolved oxygen in DI-water. Therefore, for every experiment, fresh copper nanofluid is prepared. Three different concentrations (0.057%, 0.1%, and 0.2%) of copper nanofluid are prepared to compare the results with graphene and the MWCNT nanofluid.
- Silica nanofluid: Silica is chosen because of its electrically insulating property, as silica nanofluid is used to validate the effect of electrical conductivity. Therefore, only one volume fraction of silica nanofluid is prepared.
- Surfactant: To enhance the stability of nanofluid, 4 mM of sodium dodecyl sulfate (SDS) is added to the base fluid. 4 mM SDS concentration is preferred as it is half of the critical micelle concentration of SDS in DI-water.²¹ To ensure that there is no discrepancy because of the surfactant, the concentration of the surfactant in each sample of nanofluids is kept identical, i.e., 4 mM.

In the present experiment, a two-step method is used for the preparation of nanofluids, i.e., nano-particles are procured from the manufacturer and then dispersed in the base fluid. To avoid agglomeration and to obtain uniform concentration of nano-particles in the base fluid, the solution of nano-particles and surfactant in DI water is first agitated for 30 min in a magnetic stirrer followed by sonication for another 30 min.

Dynamic viscosity and thermal conductivity of nanofluids are measured, and the plots showing relative dynamic viscosity versus temperature and relative thermal conductivity versus temperature are shown in Fig. 3. It is clear from the

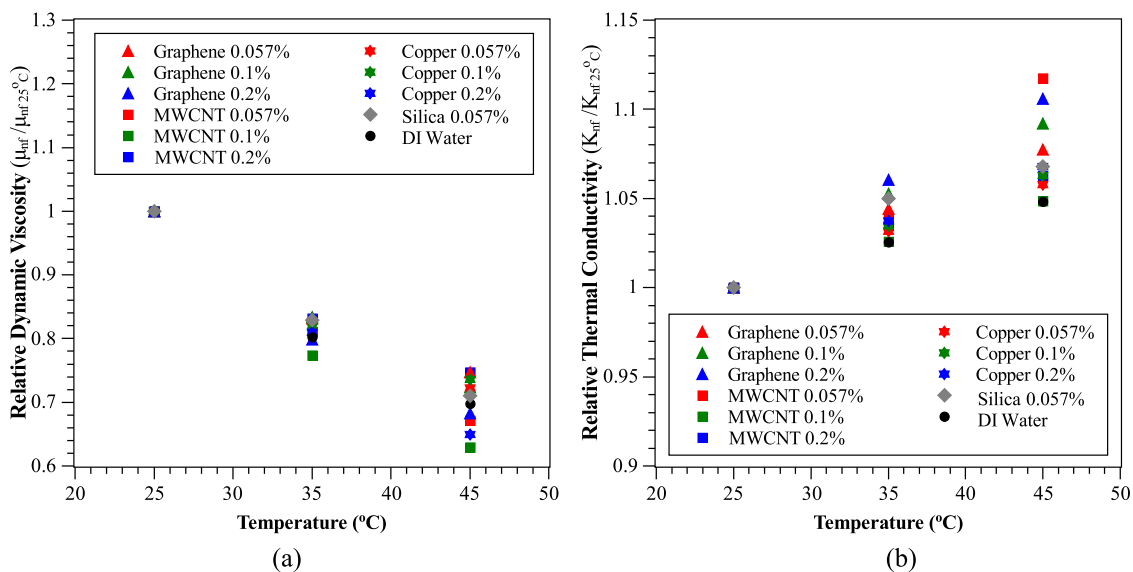


FIG. 3. (a) Relative dynamic viscosity vs temperature. (b) Relative thermal conductivity vs temperature.

plots that viscosity and thermal conductivity are strong functions of temperature. The dynamic viscosity decreases with temperature and drops by 33% (maximum) from 25 °C to 45 °C. However, the thermal conductivity increases with temperature and a maximum enhancement of 11% is observed from 25 °C to 45 °C. The dynamic viscosity of nanofluid is measured using an Anton Paar AMVn Automated Microviscometer, and thermal conductivity is measured using a KD2 Pro Thermal Property Analyzer. Properties like heat capacity, the coefficient of thermal expansion, and the density of nanofluid are calculated using correlations based on volumetric averaging²² as follows:

$$\beta_{nf} = (\phi\beta_{np}) + ((1 - \phi)\beta_{bf}), \tag{1}$$

$$\rho_{nf} = (\phi\rho_{np}) + ((1 - \phi)\rho_{bf}), \tag{2}$$

$$C_{nf}\rho_{nf} = (\phi C_{np}\rho_{np}) + ((1 - \phi)C_{bf}\rho_{bf}). \tag{3}$$

Electrical conductivity at room temperature is measured to have an overall idea of the effective electrical conductivity of the nanofluid sample. It is evident from the measurement that the electrical conductivity of the nanofluid sample is approximately negligible in comparison to the electrical conductivity of pure metals like copper ($\approx 10^7$ S/m). To quantify the stability of the nanofluids, zeta potential of samples is measured. Water based nanofluids with zeta potential less than -30 mV are considered stable.²³ The electrical conductivity and zeta potential of the samples are tabulated in Table I.

B. Heat loss calculation

A standard method used by Okada and Ozoe¹² is used to estimate heat loss, in which convection currents inside the cavity are seized by placing the hot side up and the cold side down. Therefore, the heat transfer between the hot and cold faces is mainly due to conduction through the test fluid (water) and acrylic walls. The conduction from the back of the heater and through the acrylic walls is considered as heat loss.

The heat loss (Q_{loss}) at steady state refers to the difference between the heat supplied by the electrical heater and heat conducted (Q_c) through the test fluid from the hot side to the cold side

$$Q_{loss} = Q_s - Q_c. \tag{4}$$

In the above equation, heat conducted (Q_c) from the hot side to the cold side can be estimated by one dimensional Fourier law of heat conduction and heat supplied (Q_s) to the

TABLE I. Electrical conductivity at room temperature.

Measured quantity	Concentration	σ (μ S/cm)	Zeta potential (mV)
DI water	...	7.7	...
DI water + surfactant	4 mM	128	...
MWCNT nanofluid	0.1% V/V	207.4	-37.6
Copper nanofluid	0.1% V/V	245.8	-34.7
Graphene nanofluid	0.1% V/V	273.8	-49.1

heater is just the product of current through and voltage across the heater

$$Q_c = \frac{k_w A(\Delta T)}{L}, \tag{5}$$

$$Q_s = VI. \tag{6}$$

Therefore,

$$Q_{loss} = VI - \frac{k_w A(\Delta T)}{L}. \tag{7}$$

After repeating the experiment with different values of power input, a linear correlation between Q_{loss} and ΔT is developed, which is used to estimate heat loss in the experiment

$$Q_{loss} = 0.0615(\Delta T) + 0.0121. \tag{8}$$

Figure 4 shows the plot of heat loss versus heat supplied at different ΔT for one of the cases in the present experiment. The heat loss varies from 18% to 26% of the heat supplied. In experiments, the ambient temperature is maintained between 25 °C and 26.5 °C.

C. Validation of experimental setup and procedure

In order to validate the experimental procedure and setup, a set of experiments with DI-water as test fluid is carried out and the experimentally calculated Nusselt number is compared with the Nusselt number computed in simulations done on ANSYS FLUENT 17.2 (a similar experimental study with water as test fluid is not available in the literature). A three-dimensional steady-state simulation is carried-out with exactly the same experimental cavity dimensions,

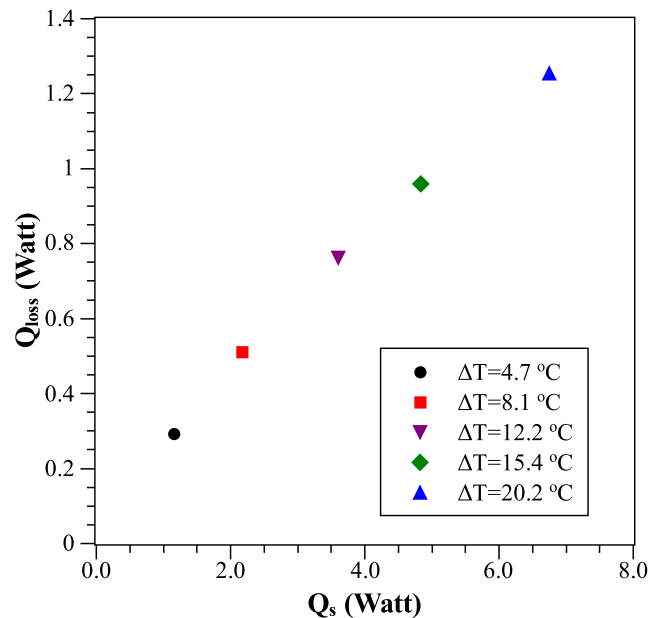


FIG. 4. Heat-loss versus heat-supplied at the observed temperature difference.

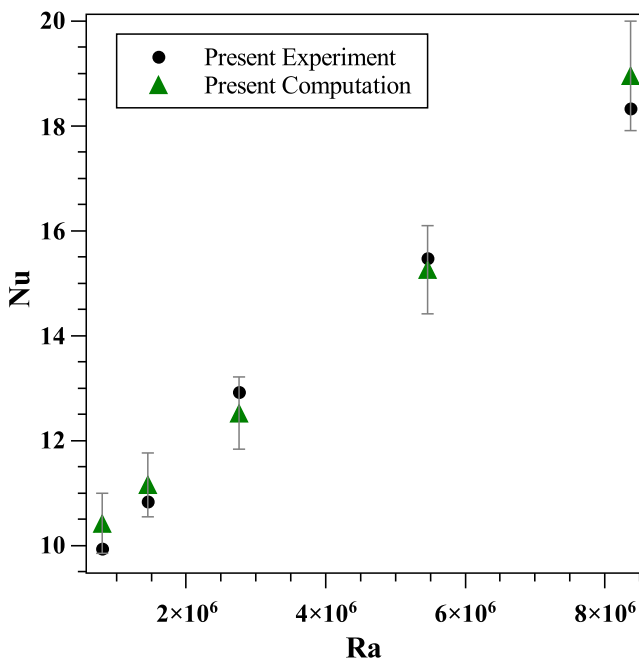


FIG. 5. Comparison between the present experiment and computation with water as test fluid.

i.e., 25 mm × 25 mm × 25 mm and boundary conditions—two opposite faces being at two different constant temperatures and the rest four faces being adiabatic. The whole cavity is divided into 100 × 100 × 100 uniformly spaced mesh points. The temperature of the hot and the cold plates in simulations is kept the same as measured in experiments, i.e., an average temperature of five thermocouples placed on each hot and cold side. The experimental results (Ra , Nu) are then compared with the corresponding Fluent simulation results (Ra , Nu).

A comparison between both results is shown in Fig. 5. The computational results for the Nusselt number and the Rayleigh number are found to be in good agreement with the corresponding experimental measured values within the uncertainty limit.

The agreement of computational and experimental results validates the experimental procedure, the heat-loss method, and the experimental setup within the measurement uncertainty limit of this experiment.

To validate the computational solver—simulations with air as test fluid are run for cases available in the literature,²⁴ and a comparison between the results is shown in Fig. 6.

The present computation is in agreement with the results of Fusegi *et al.*,²⁴ which validates the solver used in this study to validate the experimental setup and heat loss method. The average uncertainty in the Nusselt number is 5.5% and the Rayleigh number is 3.0% (see the Appendix).

III. RESULTS AND DISCUSSION

A. MWCNT nanofluid

To elicit the effect of the direction and the strength of the magnetic field, first few experiments are conducted with the MWCNT (0.057%) nanofluid as test fluid under two different magnetic field directions (X and Y) as shown in Fig. 7 and at two different magnetic field strengths (0.13 T and 0.3 T).

In the presence of the magnetic field (0.3 T, Y-direction), the heat transfer in the MWCNT (0.057%) nanofluid is found to be depreciated by an average 8.0% over the considered Rayleigh number range (1×10^6 to 1×10^7) as shown in Fig. 8.

However, magnetic field (0.13 T in the X-direction) impeded the heat transfer rate in the MWCNT (0.057%) nanofluid by an average of 8.4% over the considered Rayleigh number range with a maximum depreciation of 11.3% at a lower Rayleigh number (1×10^6), with an increase in the

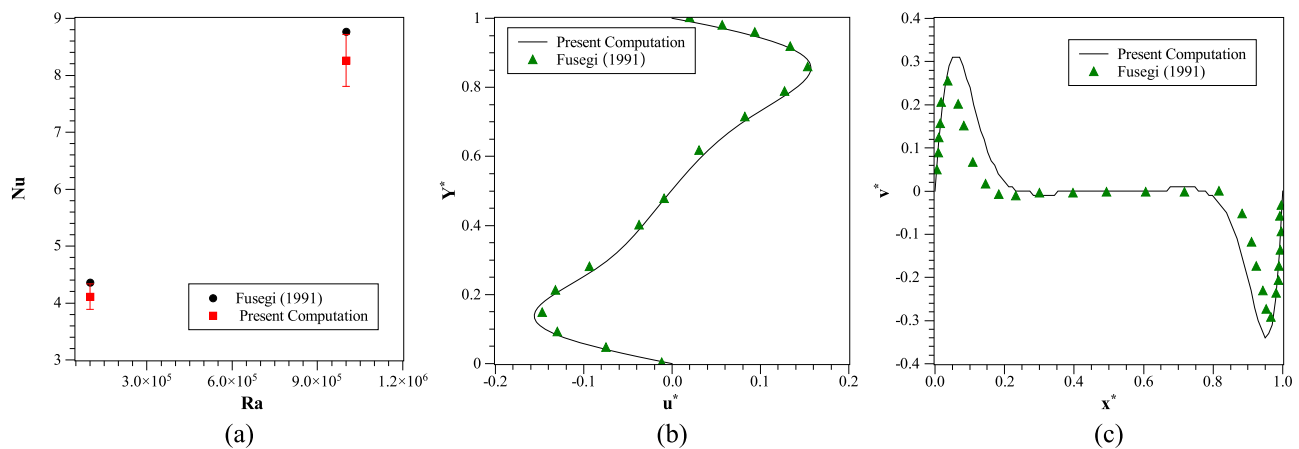


FIG. 6. Comparison of the present computation with Fusegi *et al.*²⁴'s result (test fluid as air). (a) Nu vs Ra plot, (b) non-dimensional u velocity vs non-dimensional Y coordinate at $Z^* = 0.5$, and (c) non-dimensional V velocity vs non-dimensional X coordinate at $Z^* = 0.5$.

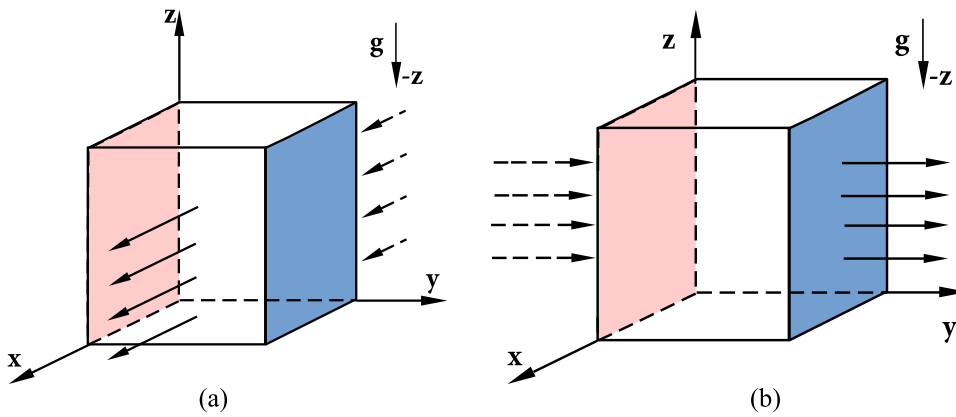


FIG. 7. Magnetic field lines with respect to the heater and condenser walls. (a) X-direction magnetic field and (b) Y-direction magnetic field. Red—heater face, blue—condenser face, and arrow—direction of the magnetic field.

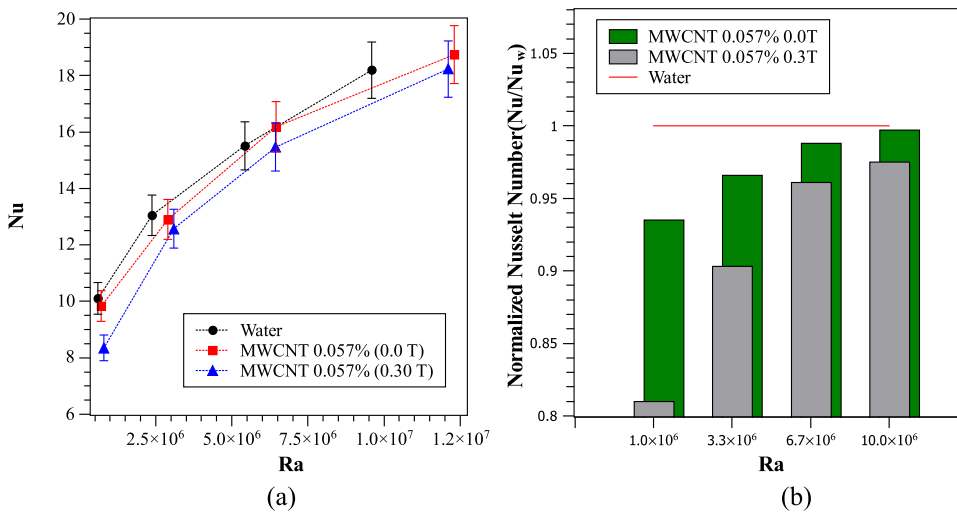


FIG. 8. (a) Nu vs Ra plot, (b) normalized Nu vs Ra—for MWCNT 0.057% nanofluid, Y-direction magnetic field.

magnetic field strength to 0.3 T in the X-direction, and the heat transfer rate in the MWCNT (0.057%) nanofluid is observed to be depreciated by an average of 12.0% over the considered Rayleigh number range with a maximum of 16.0% at lower a Rayleigh number (1×10^6). Higher average reduction with the X-direction magnetic field can be attributed to a greater Lorentz force on particles as entire convection current in the cavity is perpendicular to the magnetic field lines as shown in Fig. 9(a).

The magnetic field lines are perpendicular to the convection current, i.e., velocity components at all points on the convection loop, for example, at points 1, 2, 3, and 4. However, in the Y-direction magnetic field, the convection currents are perpendicular to the flow only when the flow is rising near the heater plate and when it is plummeting near the condenser plate as shown in Fig. 9(b); in this case, the magnetic field lines are perpendicular to one component of velocity and is parallel to the other; for example, at points 4 and 2, magnetic field lines are perpendicular, while at points 1 and 3, it is parallel. A detailed mathematical explanation is provided in Sec. IV.

In the absence of magnetic field, the MWCNT (0.057%) nanofluid showed a small depreciation of 7.0% (maximum at a lower Rayleigh number) and 3.0% (average over the considered Rayleigh number range), which can be attributed to the trade-off between the increased viscosity—which

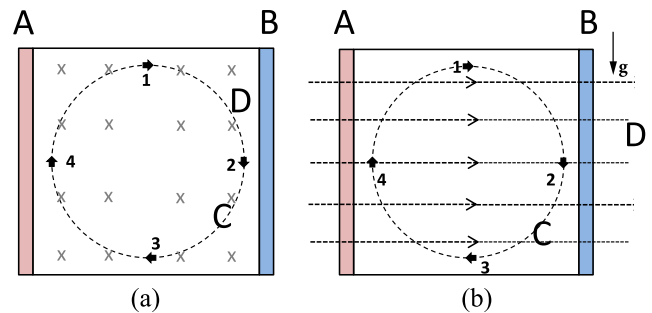


FIG. 9. Relative orientation of convection current with the magnetic field. (a) Magnetic field X direction and (b) magnetic field Y direction. A—heater plate, B—condenser plate, C—convection current, and D—magnetic field lines.

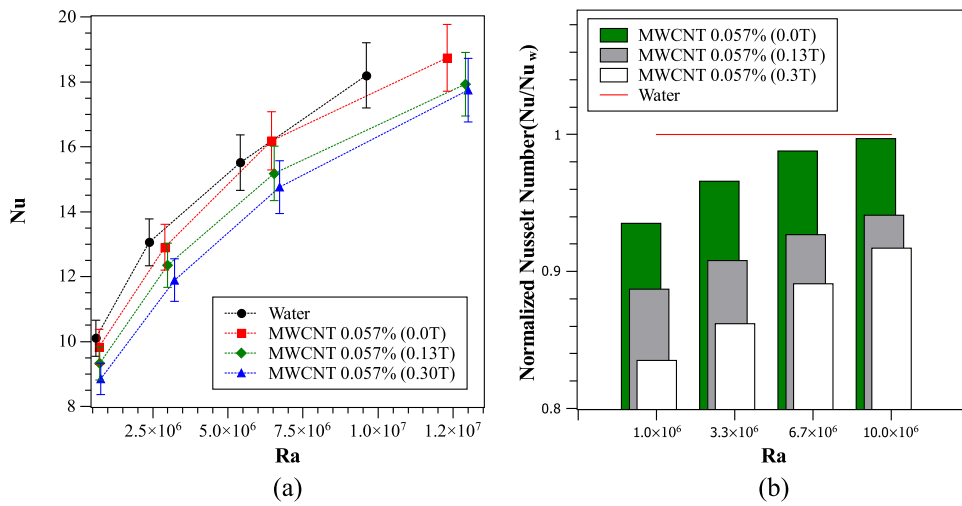


FIG. 10. (a) Nu vs Ra plot and (b) normalized Nu vs Ra—for MWCNT 0.057% nanofluid, X-direction magnetic field.

reduces the heat transfer as buoyancy effect is reduced and increased thermal conductivity because of which heat transfer increases.

As the depreciation in heat transfer is more when the magnetic field is in the X-direction, therefore further experiments with remaining nanofluids are carried out with the magnetic field in the X-direction.

The MWCNT (0.1%) nanofluid shows an enhancement of 7.0% (average, for the considered Rayleigh number range) and 12.0% (maximum, at a lower Rayleigh number) in heat transfer with respect to the DI-water. However, on the application of magnetic field (0.3 T, X-direction), the enhanced heat transfer rate is observed to be suppressed by a maximum of 7.0% with an average of 4.0% over the considered Rayleigh number range, as shown in Fig. 11.

The depreciation at a lower Rayleigh number ($\approx 10^6$) is clearly seen for MWCNT 0.057% (0.3 T, X and Y directions)

and MWCNT 0.1% with certainty in Figs. 8, 10, and 11, while at a higher Rayleigh number, the depreciation is low and within the uncertainty limit of experiments as the effect of magnetic field is gradually diminishing with increasing Rayleigh number.

The MWCNT (0.2%) nanofluid shows deterioration in heat transfer with respect to DI-water in the absence of magnetic field, which is further depreciated on the application of magnetic field, but the deterioration is not found to be significant as shown in Fig. 12.

Therefore, the deteriorating effect of magnetic field on heat transfer is observed to be diminishing with an increase in volume fraction as for the MWCNT (0.057%) nanofluid, the average deterioration is 12%, for the MWCNT (0.1%) nanofluid, the average deterioration is 7.0%, and for the MWCNT (0.2%) nanofluid, the average deterioration is 3.0%. The enhancement in heat transfer is seen only for 0.1% MWCNT nanofluid,

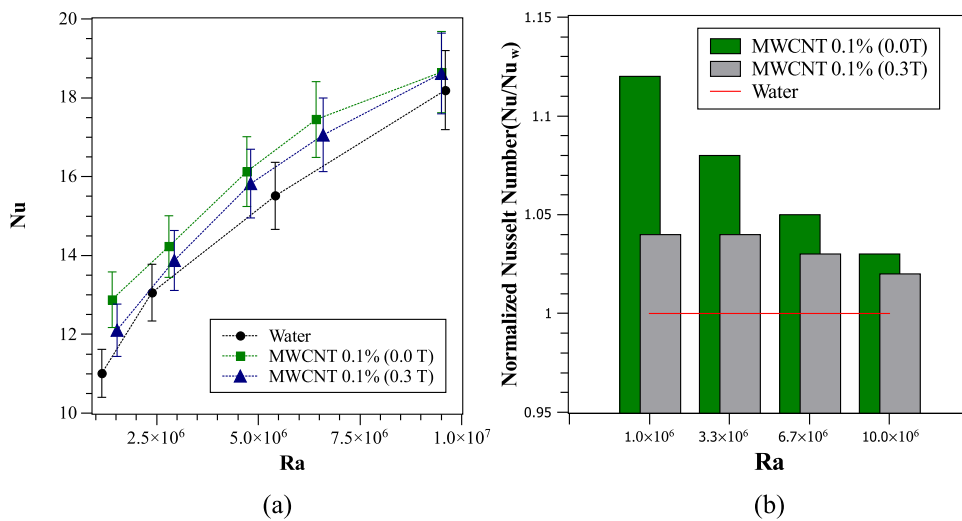


FIG. 11. (a) Nu vs Ra plot and (b) normalized Nu vs Ra—for MWCNT 0.1% nanofluid, X-direction magnetic field.

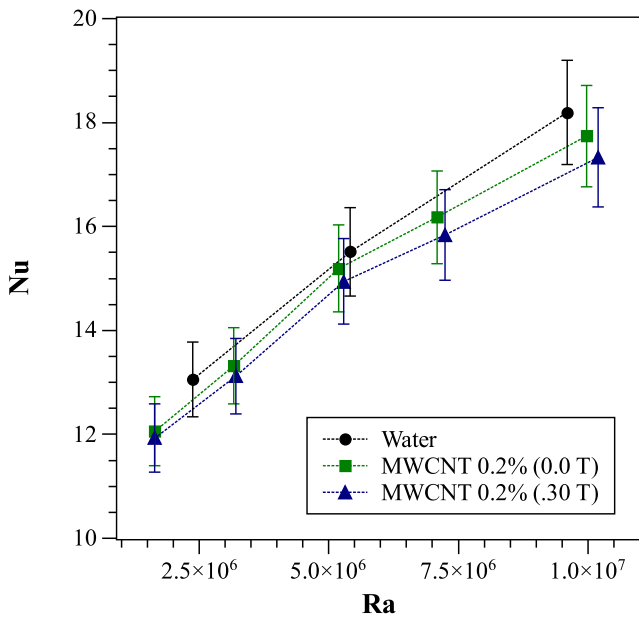


FIG. 12. Nu vs Ra plot for MWCNT 0.2% nanofluid, X-direction magnetic field.

while both 0.057% and 0.2% MWCNT nanofluids show depreciation with respect to DI-water. Therefore, the presence of an optimum volume fraction is thus justified.⁹ Every experiment is repeated at least 3 times in a span of 2 days, and the results were well within the uncertainty limit of the experiment.

B. Graphene nanofluid

With the use of graphene (0.057%) nanofluid as test fluid, the heat transfer is found to be enhanced by an average 7.0% over the considered Rayleigh number range and a maximum of 13% at lower values of Rayleigh number (1×10^6) in the absence

of magnetic field. The extent of enhancement in heat transfer is found to be diminishing with an increase in the Rayleigh number.

The enhanced heat transfer is observed to be deteriorated in the presence of magnetic field, and the heat transfer is deteriorated by 6.6% (average, over the considered Rayleigh number range) and 14.0% (maximum, at lower values of Rayleigh number). The effect of magnetic field on heat transfer suppression is also found to be diminishing with an increase in the Rayleigh number as shown in Fig. 13.

In the absence of magnetic field, an enhancement in heat transfer is also observed for graphene (0.1%) and graphene (0.2%) nanofluids. Graphene (0.1%) nanofluid showed an average enhancement in heat transfer of 10%, and graphene (0.2%) nanofluid showed an average enhancement of 5.0% in heat transfer, while the maximum enhancement in the considered Rayleigh number is found to be 16.0% and 8.0% for graphene (0.1%) and graphene (0.2%) nanofluids, respectively, at lower values of Rayleigh number (1×10^6). As expected, in the presence of magnetic field, both samples of nanofluid showed deterioration in heat transfer with the Nusselt number being suppressed by an average of 7.9%, maximum depreciation being 11.8% for graphene (0.1%) nanofluid, and an average of 5.4% with a maximum of 17.3% at a lower Rayleigh number for graphene (0.2%) nanofluid as shown in Figs. 14(b) and 15(b).

C. Copper nanofluid

In the absence of magnetic field, copper 0.057%, 0.1%, and 0.2% nanofluids show similar heat transfer characteristics as DI-water. Moreover, deterioration for all volume fractions of copper nanofluid in the presence of magnetic field is found to be indiscernible as shown in Fig. 16, even after copper has a finite electrical conductivity of 5.96×10^7 S/m.

The Lorentz force on a moving particle in a given magnetic field depends on the volume and the electrical conductivity of the particle. Therefore, even after the copper

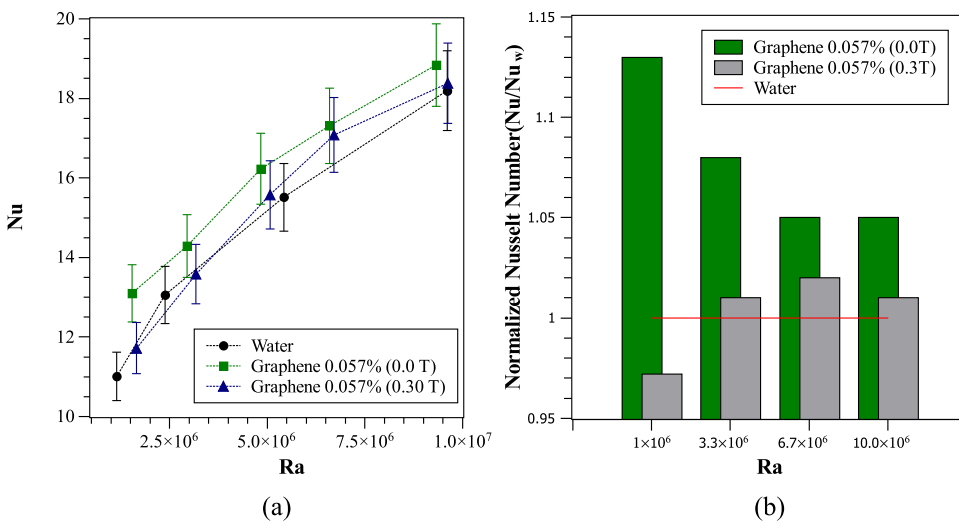


FIG. 13. (a) Nu vs Ra plot and (b) normalized Nu vs Ra—for graphene 0.057% nanofluid, X-direction magnetic field.

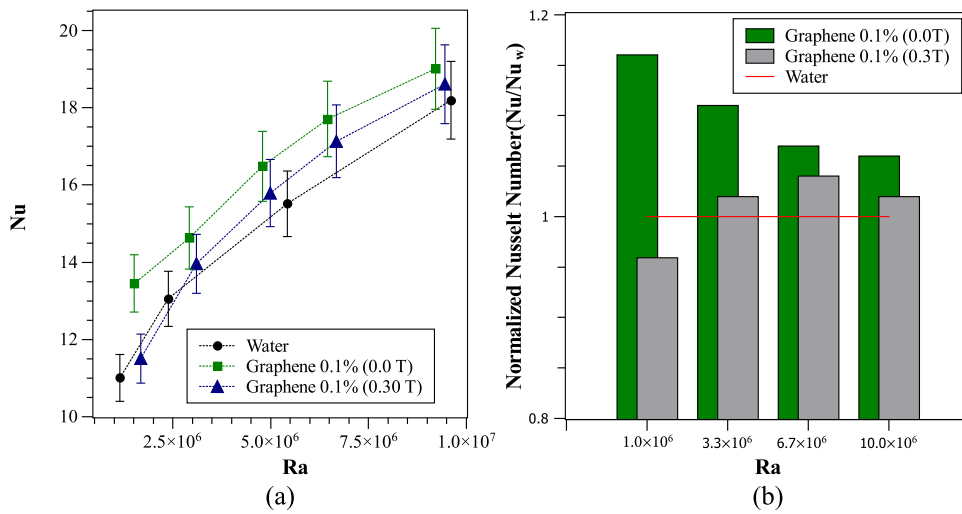


FIG. 14. (a) Nu vs Ra plot and (b) normalized Nu vs Ra—for graphene 0.1% nanofluid, X-direction magnetic field.

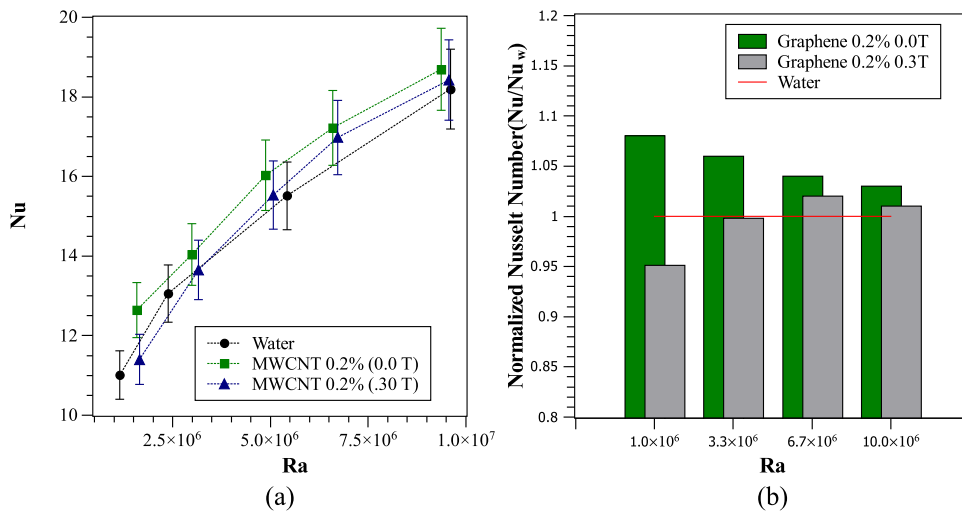


FIG. 15. (a) Nu vs Ra plot and (b) normalized Nu vs Ra—for graphene 0.2% nanofluid, X-direction magnetic field.

nano-particle has a finite electrical conductivity, it is unaffected by the external magnetic field. A detail explanation on the dependence of Lorentz force on electrical conductivity and volume of particle is provided in Sec. IV.

D. Silica nanofluid

To verify the role of electrical conductivity, experiments with 0.057% silica (electrical insulator) nanofluid are conducted at variable strengths of magnetic field, i.e., 0.12 T and 0.3 T, as shown in Fig. 17. The magnetic field (0.12 T and 0.3 T) has no effect on the heat transfer in silica 0.057% nanofluid at all as expected. All the curves (0.0 T, 0.12 T, and 0.3 T) on the Nu vs Ra plot overlapped each other.

The role of surfactant in depreciation of heat transfer is also ruled out as all volume fractions of silica nanofluid have the same concentration of SDS 4 mM, suggesting that the effect of magnetic field is only felt when particles are electrically conducting.

IV. HEAT TRANSFER DEPRECIATION MECHANISM

The mechanism behind the depreciation of heat transfer in the presence of magnetic field can be attributed to the Lorentz force (drag force) on the particles, which comes into play because of motion of electrically conducting particles in the magnetic field with velocity components perpendicular to the magnetic field.²⁵ An electric field is induced in the particle due to its motion in the magnetic field. The induced electric field at any point on the particle moving with velocity \vec{v} in a magnetic field \vec{B} is mathematically given by the equation

$$\vec{E} = \vec{v} \times \vec{B}. \tag{9}$$

The induced electric field engenders a current density in the particle given by

$$\vec{J} = \sigma \vec{E}. \tag{10}$$

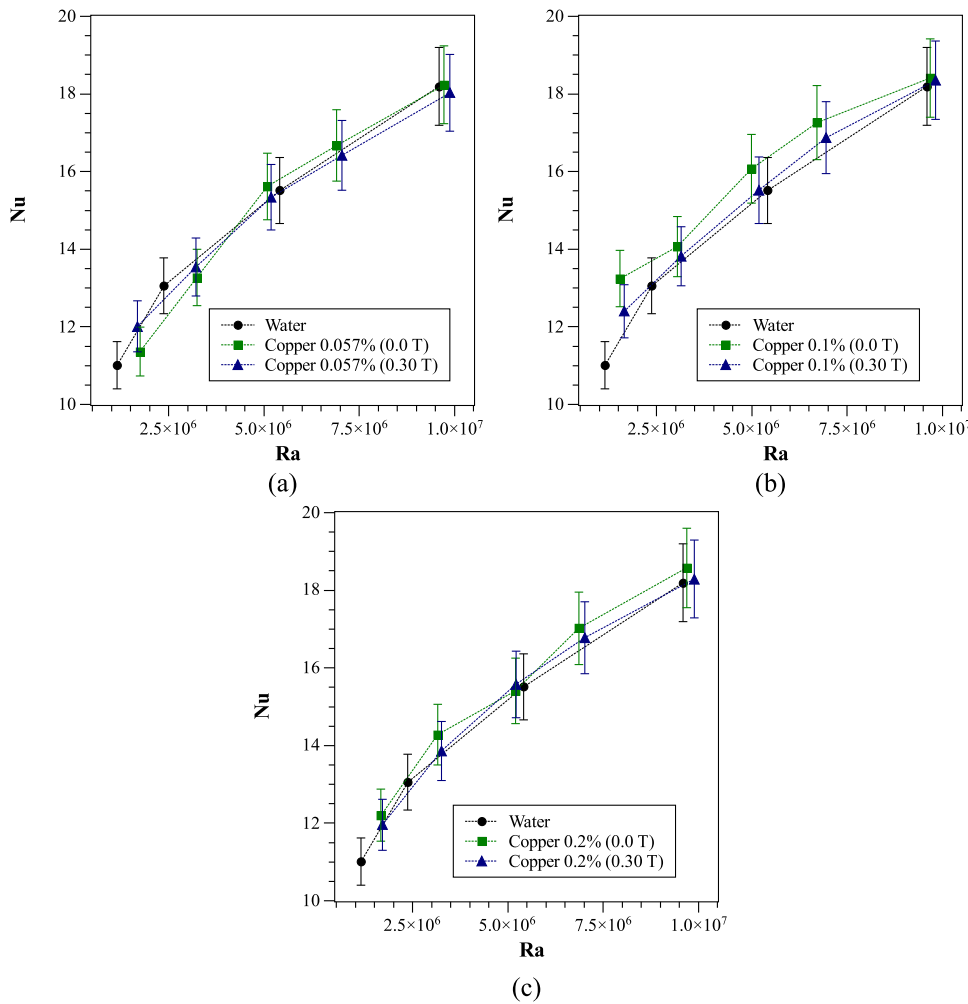


FIG. 16. Nu vs Ra plot for (a) copper 0.057% nanofluid, (b) copper 0.1% nanofluid, and (c) copper 0.2% nanofluid, X-direction magnetic field.

The current density \vec{J} gives rise to the Lorentz force \vec{F} given by the integral over the volume Ω

$$\vec{F} = \int (\vec{J} \times \vec{B}) \partial\Omega. \tag{11}$$

Consider σ , \vec{B} , and \vec{V} uniform over the volume. Therefore,

$$\vec{F} = -\sigma[(\vec{B} \cdot \vec{B})\vec{V} - (\vec{B} \cdot \vec{V})\vec{B}]\Omega. \tag{12}$$

Considering the following Cartesian coordinate system:

CASE 1: The magnetic field is along the X-axis ($\vec{B} = B_x \hat{i}$)

$$\vec{F}_y = -\sigma B_x^2 V_y \Omega, \tag{13}$$

$$\vec{F}_z = -\sigma B_x^2 V_z \Omega. \tag{14}$$

CASE 2: The magnetic field is along the Y-axis ($\vec{B} = B_y \hat{j}$)

$$\vec{F}_x = -\sigma B_y^2 V_x \Omega, \tag{15}$$

$$\vec{F}_z = -\sigma B_y^2 V_z \Omega. \tag{16}$$

The negative sign in force \vec{F} shows that it acts in opposite direction to the perpendicular velocity components and hence drags the particle. The Lorentz force (drag force) on the particle is directly proportional to the volume of the particle (Ω), square of the magnetic field (\vec{B}), velocity component of the particle perpendicular to the magnetic field, and electrical conductivity of the particle (σ). Therefore, in case-1, \vec{F} damps the Y and Z components of velocity, while in case-2, it damps the velocity components in the X and Z directions as shown in Fig. 18.

In the present experimental study, the magnetic field's direction and strength is constant. Therefore, the relative magnitude of force on MWCNT, graphene, and copper nano-particles is determined by the product of volume and electrical conductivity of the particle ($\sigma \cdot \Omega$) for a given velocity field. Comparative data for MWCNT, graphene, and copper nano-particles are tabulated in Table II. The relative force on particles with respect to the MWCNT nano-particle ($\sigma \cdot \omega / (\sigma \cdot \omega_{MWCNT})$) in the fourth column clearly suggests that the magnitude of Lorentz force is maximum for the MWCNT

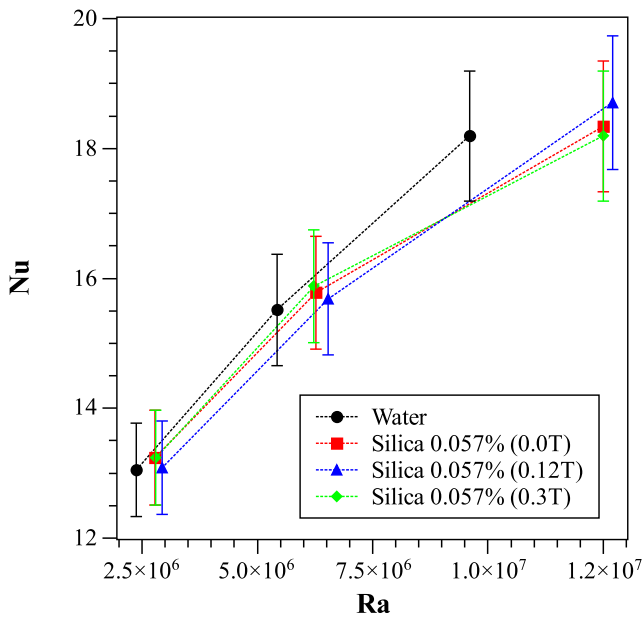


FIG. 17. Nu vs Ra plot for silica 0.057%, 0.1%, and 0.2% nanofluid, X-direction magnetic field.

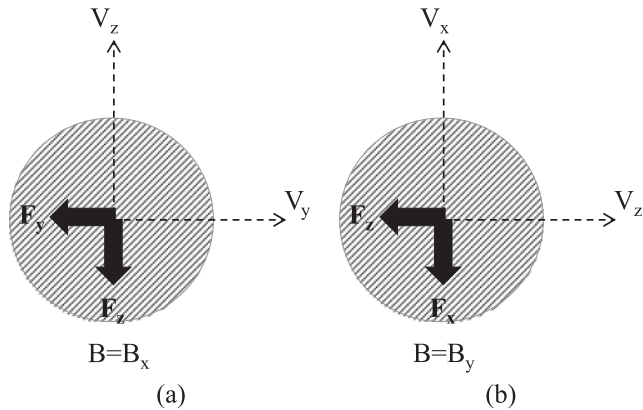


FIG. 18. Component of Lorentz force: (a) magnetic field is along the X axis and (b) magnetic field is along the Y axis.

particle, while the magnitude of Lorentz force for copper and graphene is 10^4 and 10 times lesser than MWCNT, respectively. The average deterioration in heat transfer for MWCNT

(0.057%) and graphene (0.057%) in the presence of magnetic field (0.3 T, X-direction) is 12.0% and 6.6%, respectively, while the deterioration in copper (0.057%) and silica (0.057%) is nearly discernible or approximately zero. Therefore, the experimental results are in agreement with the theory.

The explanation behind the difference in heat transfer deterioration because of the magnetic field direction (X and Y) is that, when the magnetic field is along the X axis (\vec{B}_x), the components of Lorentz force \vec{F}_y, \vec{F}_z decelerate both \vec{V}_y, \vec{V}_z velocities, respectively. However, when the magnetic field is along the Y-axis (\vec{B}_y), the components of Lorentz force \vec{F}_x, \vec{F}_z decelerate \vec{V}_x (X component of velocity being very small), \vec{V}_z velocities, respectively, while the parallel component of velocity \vec{V}_y encounters zero deceleration. As in the latter case, only \vec{V}_z encounters deceleration out of the two major components of velocities \vec{V}_y, \vec{V}_z which implies overall less drag. Therefore, the deterioration in heat transfer is less as compared to the prior case.

Net Lorentz force in case 1 ($\vec{B} = \vec{B}_x$):

$$F_{net1} = \sqrt{(\vec{F}_y)^2 + (\vec{F}_z)^2}, \tag{17}$$

$$F_{net1} = \sqrt{(-\sigma B_x^2 V_y \Omega)^2 + (-\sigma B_x^2 V_z \Omega)^2}. \tag{18}$$

Net Lorentz force in case 2 ($\vec{B} = \vec{B}_y$):

$$F_{net2} = \sqrt{(\vec{F}_x)^2 + (\vec{F}_z)^2}, \tag{19}$$

$$F_{net2} = \sqrt{(-\sigma B_y^2 V_x \Omega)^2 + (-\sigma B_y^2 V_z \Omega)^2}, \tag{20}$$

$$\begin{aligned} \text{As } \vec{V}_z \gg \vec{V}_x \\ \therefore F_{net2} = \sqrt{(-\sigma B_y^2 V_z \Omega)^2}. \end{aligned} \tag{21}$$

From Eqs. (18) and (21), $F_{net2} < F_{net1}$.

Figures 19 and 20 show the direction of velocity (taken from simulation with water as test fluid for representation) and Lorentz force [calculated using Eqs. (18) and (20)] with the relative magnitude of Lorentz force on a MWCNT, graphene, and copper nano-particle when the magnetic field is in the X-direction and Y-direction, respectively. In Figs. 19(a) and 19(b), the Lorentz force decelerates both \vec{V}_y, \vec{V}_z velocities as the magnetic field is perpendicular to both the components of velocity, while Fig. 20 shows that the Lorentz force

TABLE II. Comparison of Lorentz force on particles.

Particle (shape)	Dimension of the particle	σ	$\sigma \cdot \omega / (\sigma \cdot \omega_{MWCNT})$
MWCNT (tubular)	OD(20–30 nm), Length \approx (10 μ m)	5×10^7	1
Graphene (flake)	$D \approx 1 \mu$ m, Thickness \approx (1.6 nm)	10^8	1.28×10^{-1}
Copper (spherical)	$D \approx 25$ nm	5.96×10^7	4.97×10^{-4}
Silica (spherical)	$D \approx 25$ nm	$\approx 10^{-18}$	$\approx 10^{-29}$

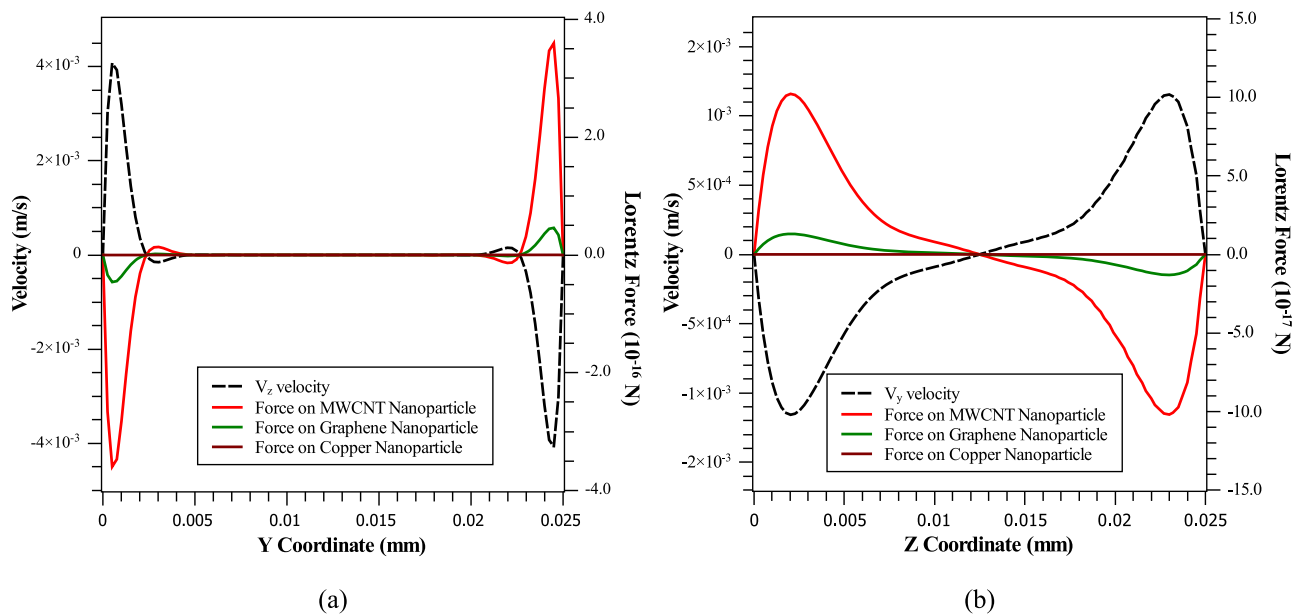


FIG. 19. (a) \vec{V}_z and \vec{F}_z along the horizontal line (middle) on the $X = 12.5$ mm plane; (b) \vec{V}_y and \vec{F}_y along the vertical line on the $X = 12.5$ mm plane ($\vec{B} = B_x \hat{i}$).

is present in Fig. 20(a) and is absent in Fig. 20(b) as the magnetic field \vec{B}_y is perpendicular and parallel to the \vec{V}_z and \vec{V}_y , respectively.

The Lorentz force is maximum for the MWCNT particle followed by graphene and then Copper. The silica nano-particle has electrical conductivity of order 10^{-18} S/m; therefore, the overall Lorentz force on silica particle is very

small and thus the heat transfer for silica remains unaffected by the presence of magnetic field.

The electrically conducting nano-particle suspensions have potential applications like MRI and nuclear-reactor cooling. In such applications, the flow of nanofluid can interact with the magnetic field which will produce a deteriorating effect on the heat transfer.

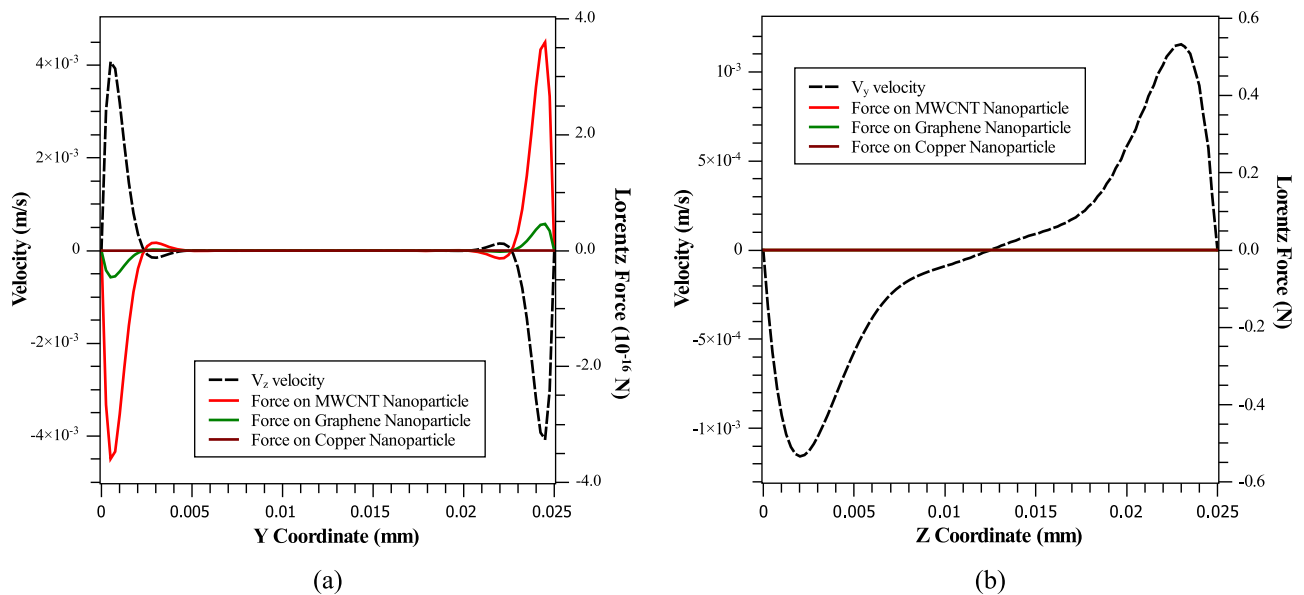


FIG. 20. (a) \vec{V}_z and \vec{F}_z along the horizontal line on the $X = 12.5$ mm plane; (b) \vec{V}_y and \vec{F}_y along the vertical line (middle) on the $X = 12.5$ mm plane ($\vec{B} = B_y \hat{j}$).

V. CONCLUSIONS

The effect of an external magnetic field on natural convection in differentially heated cubical cavity is experimentally investigated. Deterioration in heat transfer behavior of electrically conducting, non-magnetic nano-particle suspension clearly shows that an external magnetic field can perturb the heat transfer characteristics if particles are electrically conducting. The deterioration in heat transfer is found to be varying with the direction, strength of the magnetic field, type of nanofluid, concentration of nanofluid, and Rayleigh number. The MWCNT nanofluid shows the maximum depreciation in heat transfer followed by graphene and copper nanofluid. The heat transfer rate in silica nanofluid is unaffected by the presence of magnetic field as the deterioration in heat transfer is determined by the product of electrical conductivity and volume of the particle ($\sigma \cdot \omega$) for a given magnetic field and velocity field. The deterioration in MWCNT nanofluid is found to be more when the magnetic field is along the X-direction as compared to the Y-direction magnetic field. This is attributed to the Lorentz force on the particle in the former case which decelerates both the major components of velocity \vec{V}_y and \vec{V}_z . With increasing magnetic field strength from 0.12 T to 0.3 T, the deterioration in heat transfer for MWCNT is observed to be greater, as the Lorentz force is directly proportional to the square of magnetic field strength. With the increasing volume fraction of nanofluid, the deterioration in heat transfer in the presence of magnetic field is seen to be diminishing in MWCNT and graphene—the heat transfer deterioration is maximum for 0.057% volume fraction followed by 0.1% and than 0.2%. With an increase in the Rayleigh number, the percentage deterioration in the heat transfer in the presence of the magnetic field is found to get diminished. At a lower Rayleigh number, maximum deterioration is found to be 19% for the MWCNT (0.057%) nanofluid, which decreases with increasing Rayleigh number. Heat transfer in nanofluid

in the absence of magnetic field is found to be enhanced for graphene nanofluids (0.057%, 0.1%, and 0.2%), and 10% enhancement in heat transfer is observed for the graphene 0.1% nanofluid. The enhancement in heat transfer in MWCNT nanofluid in the absence of magnetic field is observed only at 0.1% volume fraction. The copper nanofluid shows heat transfer characteristics similar to those of DI-water.

APPENDIX: UNCERTAINTY ANALYSIS

The uncertainty in the measurement of various measurable quantities used in the calculation of Nusselt and Rayleigh numbers is tabulated in Table III.

The uncertainties in the Rayleigh number and the Nusselt number are calculated as follows:

$$Ra = \frac{g\beta_{nf} \Delta TL^3}{\nu_{nf}\alpha_{nf}}, \tag{A1}$$

$$Nu = \frac{hL}{k_{nf}}, \tag{A2}$$

where

$$\alpha_{nf} = \frac{k_{nf}}{\rho_{nf}C_{nf}}, \tag{A3}$$

$$\nu_{nf} = \frac{\mu_{nf}}{\rho_{nf}}, \tag{A4}$$

$$h = \frac{VI - Q_{loss}}{A \Delta T}, \tag{A5}$$

$$Ra = Ra(\beta_{nf}, \Delta T, \rho_{nf}, k_{nf}, C_{nf}, \mu_{nf}, L,), \tag{A6}$$

$$Nu = N(h, L, k_{nf}), \tag{A7}$$

$$\sigma_{Ra} = \sqrt{\left(\frac{\partial Ra}{\partial \beta_{nf}} \sigma_{\beta_{nf}}\right)^2 + \left(\frac{\partial Ra}{\partial \Delta T} \sigma_{\Delta T}\right)^2 + \left(\frac{\partial Ra}{\partial L} \sigma_L\right)^2 + \dots + \left(\frac{\partial Ra}{\partial k_{nf}} \sigma_{k_{nf}}\right)^2 + \left(\frac{\partial Ra}{\partial C_{nf}} \sigma_{C_{nf}}\right)^2}, \tag{A8}$$

$$\sigma_{Nu} = \sqrt{\left(\frac{\partial Nu}{\partial h} \sigma_h\right)^2 + \left(\frac{\partial Nu}{\partial L} \sigma_L\right)^2 + \left(\frac{\partial Nu}{\partial k_{nf}} \sigma_{k_{nf}}\right)^2}. \tag{A9}$$

TABLE III. Uncertainties in measurement.

Measured quantity	Uncertainty	Unit
Current	0.01	A
Voltage	0.1	V
Temperature	0.1	K
Viscosity	3.0%	m Pa s
Thermal conductivity	5.0%	W/m K

REFERENCES

¹S. U.-S. Choi, "Nanofluid technology: Current status and future research," Technical Report No. ANL/ET/CP-97466, Argonne National Laboratory, Argonne, IL, USA, 1998.
²P. Nagarajan, J. Subramani, S. Suyambazhahan, and R. Sathyamurthy, "Nanofluids for solar collector applications: A review," *Energy Procedia* **61**, 2416–2434 (2014).
³M. Bahiraei and S. Heshmatian, "Electronics cooling with nanofluids: A critical review," *Energy Convers. Manage.* **172**, 438–456 (2018).
⁴T. R. Barrett, S. Robinson, K. Flinders, A. Sergis, and Y. Hardalupas, "Investigating the use of nanofluids to improve high heat flux cooling systems," *Fusion Eng. Des.* **88**(9-10), 2594–2597 (2013).
⁵S. P. Jang and S. U. Choi, "Free convection in a rectangular cavity (Benard convection) with nanofluids," in *ASME 2004 International Mechanical*

Engineering Congress and Exposition (American Society of Mechanical Engineers, 2004), pp. 147–153.

- ⁶A. A. Nnanna, T. Fistrovich, K. Malinski, and S. Choi, “Thermal transport phenomena in buoyancy-driven nanofluids,” in *ASME 2004 International Mechanical Engineering Congress and Exposition* (American Society of Mechanical Engineers, 2004), pp. 571–578.
- ⁷D. Wen and Y. Ding, “Formulation of nanofluids for natural convective heat transfer applications,” *Int. J. Heat Fluid Flow* **26**(6), 855–864 (2005).
- ⁸R. Ni, S.-Q. Zhou, and K.-Q. Xia, “An experimental investigation of turbulent thermal convection in water-based alumina nanofluid,” *Phys. Fluids* **23**(2), 022005 (2011).
- ⁹P. S. Joshi and A. Pattamatta, “Buoyancy induced convective heat transfer in particle, tubular and flake type of nanoparticle suspensions,” *Int. J. Therm. Sci.* **122**, 1–11 (2017).
- ¹⁰R. Mohebbi, M. Izadi, and A. J. Chamkha, “Heat source location and natural convection in a C-shaped enclosure saturated by a nanofluid,” *Phys. Fluids* **29**(12), 122009 (2017).
- ¹¹S. P. Schroeder and G. K. Morris, “Nanofluids in a forced-convection liquid cooling system—benefits and design challenges,” in *2010 12th IEEE Intersociety Conference on Thermal and Thermomechanical Phenomena in Electronic Systems (ITherm)* (IEEE, 2010), pp. 1–5.
- ¹²K. Okada and H. Ozoë, “Experimental heat transfer rates of natural convection of molten gallium suppressed under an external magnetic field in either the X, Y, or Z direction,” *J. Heat Transfer* **114**(1), 107–114 (1992).
- ¹³J. Joubert, M. Sharifpur, A. B. Solomon, and J. Meyer, “Enhancement in heat transfer of a ferrofluid in a differentially heated square cavity through the use of permanent magnets,” *J. Magn. Magn. Mater.* **443**, 149–158 (2017).
- ¹⁴A. Chamkha, A. Rashad, M. Mansour, T. Armaghani, and M. Ghalambaz, “Effects of heat sink and source and entropy generation on MHD mixed convection of a Cu–water nanofluid in a lid-driven square porous enclosure with partial slip,” *Phys. Fluids* **29**(5), 052001 (2017).
- ¹⁵B. Ghasemi, S. Aminossadati, and A. Raisi, “Magnetic field effect on natural convection in a nanofluid-filled square enclosure,” *Int. J. Therm. Sci.* **50**(9), 1748–1756 (2011).
- ¹⁶A. H. Mahmoudi, I. Pop, and M. Shahi, “Effect of magnetic field on natural convection in a triangular enclosure filled with nanofluid,” *Int. J. Therm. Sci.* **59**, 126–140 (2012).
- ¹⁷M. Sheikholeslami and H. B. Rokni, “Magnetic nanofluid flow and convective heat transfer in a porous cavity considering Brownian motion effects,” *Phys. Fluids* **30**(1), 012003 (2018).
- ¹⁸S. N. Shoghl, J. Jamali, and M. K. Moraveji, “Electrical conductivity, viscosity, and density of different nanofluids: An experimental study,” *Exp. Therm. Fluid Sci.* **74**, 339–346 (2016).
- ¹⁹A. Lekawa-Raus, J. Patmore, L. Kurzepa, J. Bulmer, and K. Koziol, “Electrical properties of carbon nanotube based fibers and their future use in electrical wiring,” *Adv. Funct. Mater.* **24**(24), 3661–3682 (2014).
- ²⁰B. Marinho, M. Ghislandi, E. Tkalya, C. E. Koning, and G. de With, “Electrical conductivity of compacts of graphene, multi-wall carbon nanotubes, carbon black, and graphite powder,” *Powder Technol.* **221**, 351–358 (2012).
- ²¹A. Cifuentes, J. L. Bernal, and J. C. Diez-Masa, “Determination of critical micelle concentration values using capillary electrophoresis instrumentation,” *Anal. Chem.* **69**(20), 4271–4274 (1997).
- ²²R. W. Johnson, *Handbook of Fluid Dynamics* (CRC Press, 2016).
- ²³F. Yu, Y. Chen, X. Liang, J. Xu, C. Lee, Q. Liang, P. Tao, and T. Deng, “Dispersion stability of thermal nanofluids,” *Prog. Nat. Sci.: Mater. Int.* **27**(5), 531–542 (2017).
- ²⁴T. Fusegi, J. M. Hyun, and K. Kuwahara, “A numerical study of 3D natural convection in a cube: Effects of the horizontal thermal boundary conditions,” *Fluid Dyn. Res.* **8**(5–6), 221 (1991).
- ²⁵D. Besdin, J. Shewell, and E. Ikenberry, “The motion of a conducting sphere in a uniform magnetic field,” *Am. J. Phys.* **21**(6), 418–421 (1953).